

Dynamic Phase Field Description on Ductile Fracture Process

MA Xueshi, WANG Gangyao, WANG Jia*

School of Mechanical Engineering, Jiangsu University of Science and Technology, Zhenjiang 212100, P. R. China

(Received 30 August 2024; revised 20 September 2024; accepted 10 October 2024)

Abstract: In comparison to discrete descriptions of fracture process, the recently proposed phase field methodology averts the numerical tracking strategy of discontinuities in solids, which enables the numerical implement simplification. An implicit finite element formulation based on the diffuse phase field is extended for stable and efficient analysis of complex dynamic fracture process in ductile solids. This exhibited formulation is shown to capture entire range of the characteristics of ductile material presenting J2-plasticity, embracing plasticization, cracks initiation, propagation, branching and merging while fulfilling the basic principle of thermodynamics. Herein, we implement a staggered time integration scheme of the dynamic elasto-plastic phase field method into the commercial finite element code. The numerical performance of the present advanced phase field model has been examined through several classic dynamic fracture benchmarks, and in all cases simulation results are in good agreement with the associated experimental data and other numerical results in previous literature.

Key words: implicit dynamic analysis; ductile fracture; elasto-plastic formulation; phase field; complex crack mode

CLC number: O341 **Document code:** A **Article ID:** 1005-1120(2024)05-0564-11

0 Introduction

Pursuing robust numerical methods for simulating arbitrary ductile cracks initiation and growth in solids are attracting a great attention, due to their normal existence and great importance in the structural safety design. Despite significant advances in ductile fracture simulation methodologies, consistent pursuit of efficient methods that can greatly improve the solution accuracy remains an active research topic until now.

In recent years, there are some sorts of numerical methods that may be classified into two broad groups depending on how to deal with hypothetical discontinuities: discrete versus smeared/diffuse theories. Commonly used discrete methods include the extended finite element method (X-FEM)^[1-2], generalized finite element method (G-FEM), phantom node method (PNM)^[3]. Its seminal theory enables the explicit incorporation of discontinuous displacements by adding extra nodal degrees of freedom

(DOFs). However, these methods have to define proper special data structures for tracking crack surfaces and appropriate merging of nodal DOFs associated with multiple interacting cracks. Thus, it has shown a tedious task to track the evolution of complex fracture surfaces algorithmically as well as arbitrary interacting cracks.

Another concept of fracture modeling is that the discontinuity in the cracked area is prescribed to be interpreted as smeared/diffuse damage^[4-9]. The phase-field fracture model shares several features with continuum methods, most notably with gradient-enhanced damage models, and meanwhile have recently appeared as a promising alternative to discrete formulation^[10-16]. The phase field method describes the smooth transition between the intact and fully damaged phases in a material, thus there is an advantage that it does not require to track the crack surface and path, comparing to the strong complexity of tracking crack growth in previous discrete models.

*Corresponding author, E-mail address: wjjzhh@just.edu.cn.

How to cite this article: MA Xueshi, WANG Gangyao, WANG Jia. Dynamic phase field description on ductile fracture process[J]. Transactions of Nanjing University of Aeronautics and Astronautics, 2024, 41(5):564-574.

<http://dx.doi.org/10.16356/j.1005-1120.2024.05.002>

A few very recent studies handled phase-field modeling of fracture in ductile materials. Duda et al.^[17] studied a phase field model for elasto-plastic fracture in solids. In this case, limited plastic deformation is assumed to occur in the vicinity of the crack tip. The total energy functional is considered as the sum of elastic, plastic and fracture contributions. As the ignorance of coupling between fracture and plasticity, the phase field is driven basically by the elastic strain energy density without influence from plastic contributions, leading to consistence with analyzing brittle fracture. To solve this limitation, an improved phase-field model for ductile fracture, proposed by Ambati et al.^[18], connected the propagation of the crack phase field with the accumulation of plastic strains in a thermodynamically consistent way. This proposed ductile fracture model includes two additional parameters, a threshold equivalent plastic strain and an exponent in the coupling function, which can facilitate the quantitative prediction of test results. And this phase field formulation was further extended to the three-dimensional plasticity finite strain setting^[19]. Consequently, the phase field fracture associated with the multi-surface plasticity^[20] was formulated in the variational framework for the unified yield criterion, which enables the study on different yield surfaces. Guan et al.^[21] established a three-dimensional phase-field model based on the cell-based smooth finite element method, to allow effective capturing of the evolution process of complex fracture morphology in elasto-plastic solids.

However, the elasto-plastic phase field models introduced above are developed within the static framework, which disable the fracture analysis under dynamic conditions. Thus, it is very appealing to expand the capability of elasto-plastic phase field methods into dynamic regime and to examine whether similar efficiency in numerical performance can be retained for dynamic ductile fracture issues, which is the main goal of this paper.

Consequently, the remainder of this paper is organized as follows. In Section 1, the phase field approximation for the elasto-plastic crack surface and various energy functions are stated. And then the dy-

namic formulation for elasto-plastic phase field, combined with staggered time integration scheme for fracture analysis, is detailed in Section 2. To examine numerical performance of this dynamic phase field method, Section 3 presents several representative benchmarking numerical examples. Finally, Section 4 provides the concluding remarks.

1 Elasto-Plastic Phase Field Methodology

1.1 Phase field description of the fracture surface

An internal length scale (l_c) is introduced in the principal idea of the phase-field approximation for the fracture surface. It leads to smearing the sharp crack into the regime of an elasto-plastic solid. As shown in Fig.1, we consider an arbitrary domain Ω with external boundary $\partial\Omega = \Gamma_D + \Gamma_N$ and internal discontinuity boundary Γ_d . The body is applied with a surface traction on the boundary Γ_N , and meanwhile fixed on the boundary Γ_D . Internal discontinuity Γ_d describes a set of discrete cracks. In terms of the staggered time integration scheme, it will be detailed in Section 1.3.

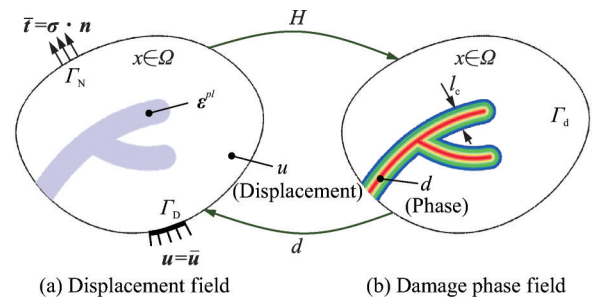


Fig.1 Illustration of the staggered scheme for elasto-plastic phase field solution in ductile solids

A damage variable $d(x)$ representing the crack phase-field function is introduced. Assume that if its value is zero, the material is intact, and while if its value reaches 1, it is fully broken. This assumption induces a smooth transition from intact to broken in ductile solids. The crack surface density function r in multiple dimensions can be defined as

$$r(d, \nabla d) = \frac{1}{2l_c} d^2 + \frac{l_c}{2} |\nabla d|^2 \quad (1)$$

where d is the damage variable and l_c length scale parameter, as mentioned above. In this approximation, the crack topology is described using the spatial gradient of the damage field. As a consequence, the volume integral of Eq.(1) over the whole domain describes the theoretical fracture surface as

$$\Gamma(d) = \int_{\Omega} r(d, \nabla d) d\Omega \quad (2)$$

where Ω is the domain of the elasto-plastic solid. It is well known that the damage variable and its gradient play a critical role in the phase field description.

1.2 Corresponding energy functional

The Lagrangian function, which describes the energy functional of the elasto-plastic dynamic issue, is expressed as

$$L(\dot{\mathbf{u}}, \mathbf{u}, d) = \Psi_{\text{kin}}(\dot{\mathbf{u}}) - \Psi_{\text{pot}}(\mathbf{u}, d) \quad (3)$$

where $\Psi_{\text{kin}}(\dot{\mathbf{u}})$ is the kinetic energy of the body, as given by

$$\Psi_{\text{kin}}(\dot{\mathbf{u}}) = \frac{1}{2} \int_{\Omega} \rho \dot{\mathbf{u}}^T \mathbf{u} d\Omega \quad (4)$$

and $\Psi_{\text{pot}}(\mathbf{u}, d)$ is the potential energy of the body, as given by

$$\Psi_{\text{pot}}(\mathbf{u}, d) = \Psi_e(\mathbf{u}, d) + \Psi_p(\mathbf{u}, d) + \Psi_f(d) \quad (5)$$

As shown in Eq.(4), $\dot{\mathbf{u}}$ is the displacement derivative and contains components of the velocity vector, and ρ the mass density. While Eq.(5) gives the total potential energy, being constructed from three components, including elastic strain energy Ψ_e , plastic strain energy Ψ_p and fracture energy Ψ_f . All components are functions of either phase field d or displacement field \mathbf{u} . Each energy component is detailed in the following subsections.

1.2.1 Elastic energy

To demonstrate the degradation of material stiffness in the fracture region (i.e., the phase-field description of the fracture surface), the elastic strain energy is defined as

$$\Psi_e(\mathbf{u}, d) = \int_{\Omega} \phi^{\text{el}}(\mathbf{u}, d) d\Omega \quad (6)$$

where ϕ^{el} is the elastic strain energy density, derived from the positive ϕ_e^+ and negative ϕ_e^- components of strain tensor. They are defined through a spectral decomposition of strain, whose detailed relations can be shown as

$$\phi^{\text{el}}(\mathbf{u}, d) = g(d) \phi_e^+(\boldsymbol{\varepsilon}^{\text{el}}(\mathbf{u})) + \phi_e^-(\boldsymbol{\varepsilon}^{\text{el}}(\mathbf{u})) \quad (7)$$

In Eq.(7), it can be seen that the material degradation under tension is involved only, instead, material remains intact under compression. And the degradation function $g(d)$ can be computed from

$$g(d) = (1 - d)^2 + k \quad (8)$$

where k is a small number responsible for the stability of the numerical solution.

For the ductile problem, an assumption can be made that the material is shear damaged equally under tension and compression. Thus, we can come into the following relation

$$\phi_e^+(\boldsymbol{\varepsilon}^{\text{el}}(\mathbf{u})) = \mu \sum_{i=1}^3 \varepsilon_i^2 + \frac{\lambda}{2} \langle \text{tr}(\boldsymbol{\varepsilon}) \rangle_+^2 \quad (9a)$$

$$\phi_e^-(\boldsymbol{\varepsilon}^{\text{el}}(\mathbf{u})) = \frac{\lambda}{2} \langle \text{tr}(\boldsymbol{\varepsilon}) \rangle_-^2 \quad (9b)$$

As known, the total strain field is divided into elastic part $\boldsymbol{\varepsilon}^{\text{el}}$ and plastic part $\boldsymbol{\varepsilon}^{\text{pl}}$.

$$\boldsymbol{\varepsilon}(\mathbf{u}) = \boldsymbol{\varepsilon}^{\text{el}}(\mathbf{u}) + \boldsymbol{\varepsilon}^{\text{pl}}(\mathbf{u}) \quad (10)$$

In this study, we only account for small deformation problem, and note that if applying the shear force under severe hydrostatic compression, the numerical result would be miscalculated due to the volumetric locking. Thus, tensile fracture cases in the ductile solids are involved only as well.

1.2.2 Plastic energy

In this subsection, we will introduce the plastic strain energy that can be expressed as

$$\Psi_p(\mathbf{u}, d) = \int_{\Omega} g(d) \psi^{\text{pl}}(\boldsymbol{\varepsilon}^{\text{pl}}(\mathbf{u})) d\Omega \quad (11)$$

where ψ^{pl} is the plastic strain energy density as a function of equivalent plastic strain ε^{pl} . Due to no permanent volumetric variation, the ductile energy history can be formulated as a function of the yield stress and the energy equivalent plastic shear strain will also be

$$\psi^{\text{pl}}(\boldsymbol{\varepsilon}^{\text{pl}}(\mathbf{u})) = \varepsilon^{\text{pl}}(\mathbf{u}) \left[\sigma_{\text{lim}}^{\text{yield}} + \frac{1}{2} \hbar \varepsilon^{\text{pl}}(\mathbf{u}) \right] + \frac{1}{2} \eta_\varepsilon \langle \varepsilon^{\text{pl}} - \varepsilon^{\text{cr}} \rangle^2 \quad (12)$$

where $\sigma_{\text{lim}}^{\text{yield}}$ is the Mises yield strength, \hbar the hardening modulus and ε^{cr} the critical equivalent plastic strain. While η_ε is a penalty parameter that induces damage when critical plastic strain is achieved. Details can be found in Ref.[22]. This implementation uses Von Mises yield criterion

$$f = \sigma^{\text{mises}} - g(d) [\sigma_{\text{lim}}^{\text{yield}} + \hbar \epsilon^{\text{pl}}] \quad (13)$$

where σ^{Mises} is the Von Mises stress, which is derived from the degraded Cauchy stress tensor. In this work, the plastic deformation experiences the same way to damage under axial compression and tension. The influence of stress triaxiality is further considered on the yield function to demonstrate the experimentally captured crack nucleation in ductile solids.

1.2.3 Fracture energy

Different from discrete fracture numerical method, the phase field simulation smears the discontinuity in solids as a continuous field to describe the material damage. Thus, the fracture energy as a function of the phase variable d can be approximated from Eq.(2) by

$$\Psi_i(d) = \int_{\Gamma} g_i d\Gamma = \int_{\Omega} \frac{g_i}{2l_c} [l_c^2 |\nabla d|^2 + d^2] d\Omega \quad (14)$$

where g_i is the unit fracture surface energy. To improve the convergence, another interesting fracture surface energy density can be introduced by providing an elastic threshold

$$\Psi_i^{\text{new}}(d) = \int_{\Omega} \phi_i [l_c^2 |\nabla d|^2 + 2d] d\Omega \quad (15)$$

where ϕ_i is the threshold parameter. In Eq.(15), the phase variable d can go to the approximation through a linear term.

2 Dynamic Staggered Time Discretization

The monolithic and staggered manners are two present strategies to account for the solution of coupled displacement and phase field matrix equations. However, the monolithic strategy tends to experience numerically unstable for the unstable crack propagation problem, especially for highly nonlinear dynamic issues. It is because this algorithm needs to search full crack paths during one iteration, which is a difficult numerical task. Accordingly, we adopt a staggered approach with history variables to couple the interaction between the displacement field and the phase field.

Fig.1 has already shown the schematic illustration of the staggered algorithm. According to the core idea of phase field methodology, the sharp

crack is smeared by the phase field driven by the force, based on the energy history from the displacement field. Conversely, the damage phase field is used for recomputing the displacement distribution. Therefore, the governing equations can be divided into two minimization problems of displacement and phase field. The displacement energy is approximated as

$$\Psi^u = \underbrace{\Psi_{\text{kin}}(\dot{\mathbf{u}}) - \Psi_e(\mathbf{u}, d) - \Psi_p(\mathbf{u}, d)}_{\text{Internal work}} + \underbrace{\int_{\Omega} \bar{\mathbf{b}} \cdot \mathbf{u} dV + \int_{\partial\Omega} \bar{\mathbf{t}} \cdot \mathbf{u} dA}_{\text{External work}} \quad (16)$$

where the external work is done by the prescribed volume $\bar{\mathbf{b}}$ and boundary $\bar{\mathbf{t}}$ tractions. By taking the variation of displacement energy, the strong form of Eulerian equations can be reformulated for the displacement field

$$\begin{cases} \nabla \sigma - \bar{\mathbf{b}} = 0 & \text{in } \Omega \\ \sigma \cdot \mathbf{n} = \bar{\mathbf{t}} & \text{on } \Gamma_N \\ \mathbf{u} = \bar{\mathbf{u}} & \text{on } \Gamma_D \end{cases} \quad (17)$$

where the displacement \mathbf{u} can be solved with the assumption of phase field d remaining constant.

In similar, the Lagrangian equation of the phase-field is formulated as

$$\Psi^d = \int_{\Omega} [g_i r(d, \nabla d) + g_i H] d\Omega \quad (18)$$

where H is the history field from the displacement, demonstrating the potential energy. To enforce the irreversibility of the damage, the history variable should satisfy the Karush-Kuhn-Tucker conditions

$$H = \begin{cases} \phi_c^+ + \phi^{\text{pl}} - \phi_i & \phi_c^+ + \phi^{\text{pl}} - \phi_i > H_n \\ H_n & \text{else} \end{cases} \quad (19)$$

where H_n is the calculated energy history at previous step n . The similar corresponding strong form for the phase field is expressed as

$$\begin{cases} \frac{g_i}{l_c} (d - l_c^2 \nabla d) = 2(1-d)H & \text{in } \Omega \\ \nabla d \cdot \mathbf{n} = 0 & \text{on } \Gamma_d \end{cases} \quad (20)$$

The basic staggered iteration process is shown in Fig.2, in which two problems of displacement and phase field are independently and simultaneously taken account based on history variables passing from the previous iteration.

In this implemented staggered scheme, the elements of these two fields are interacted through

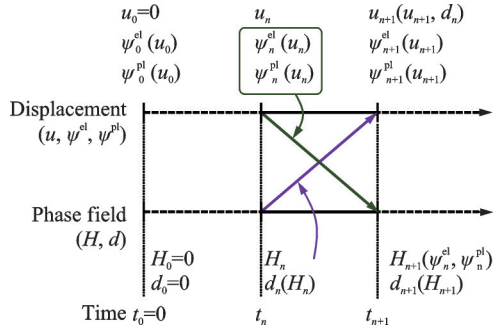


Fig.2 Staggered scheme flowchart of coupled displacement and phase field solution

only the common block. We further use the Hilber-Hughes-Taylor (HHT) method to set up a dynamic equilibrium. And then, the HHT treats the linearized equilibrium problem iteratively using the following Newton-Raphson method

$$\begin{Bmatrix} \mathbf{u} \\ \mathbf{d} \end{Bmatrix}_{n+1} = \begin{Bmatrix} \mathbf{u} \\ \mathbf{d} \end{Bmatrix}_n - \begin{bmatrix} \mathbf{\Phi}_n^u & 0 \\ 0 & (1 + \alpha) \mathbf{K}_n^d \end{bmatrix}^{-1} \begin{bmatrix} \mathfrak{R}_n^u \\ \alpha \mathfrak{R}_n^u - (1 + \alpha) \mathfrak{R}_n^d \end{bmatrix} \quad (21)$$

where \mathfrak{R}_n^u and \mathfrak{R}_n^d are the residual matrices, $\mathbf{\Phi}_n^u$ and \mathbf{K}_n^d are the element stiffness matrices of the displacement and phase field, respectively, at time t_n . The displacement tangent matrix is obtained from material stiffness \mathbf{K}_n^u and mass \mathbf{M} matrices

$$\mathbf{\Phi}_n^u = \mathbf{M} \frac{d\ddot{\mathbf{u}}}{dt} + (1 + \alpha) \mathbf{K}_n^u \quad (22)$$

where the second derivative of the displacement is defined as the following form with $\lambda = (1 - \alpha)^2/4$

$$\frac{d\ddot{\mathbf{u}}}{dt} = \frac{1}{\lambda \nabla t^2} \quad (23)$$

The displacement residual matrix can be written with an inertial component $\mathbf{f}_i^{\text{ine}}$

$$\mathfrak{R}_n^u = (1 + \alpha) \mathbf{f}_n^{\text{int}} - \alpha \mathbf{f}_{n-1}^{\text{int}} + \mathbf{f}_n^{\text{ine}} - \mathbf{f}_n^{\text{ext}} \quad (24)$$

where $\mathbf{f}_n^{\text{int}}$ and $\mathbf{f}_n^{\text{ext}}$ are the internal and external force vectors, respectively, at time t_n , and α is a damping coefficient.

For the implementation of the solution in Abaqus, a three-layer finite element structure is used as shown in Fig.3. Each layer shares the same nodes, but contributes to the stiffness of different DOFs. The elements attributed to the first layer have two or three DOFs depending on the dimensionality, while the elements in the second layer contribute to only one phase field DOF. To display the calculated quantities in post-processing, the third layer is constructed with infinitesimally small stiffness made from a UMAT (user defined material model), of which attributes are updated from the first and second layers.

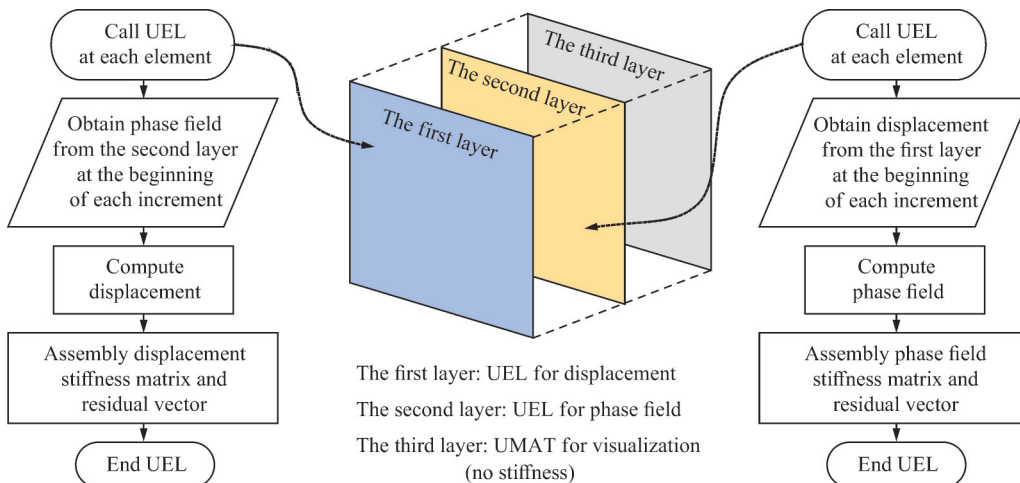


Fig.3 A three-layer finite element structure incorporated into Abaqus

3 Benchmark Numerical Examples

In this section we study the numerical performance of the dynamic phase-field fracture model to capture representative fracture characteristics in ductile

materials. The first example (dynamic ductile crack branching) aims to determine the influence of plasticity on the dynamic crack propagation patterns, and meanwhile to validate this implementation. Another example of dynamic ductile crack

propagation in an edge-cracked plate under shear loading, further illustrates the effect on numerical simulations of the presented coupling between the phase field and equivalent plastic strain.

All numerical simulations are performed within the finite element framework assuming plain strain conditions, with the material mechanical properties as shown in Table 1^[24-25].

Table 1 Material mechanical properties

Properties	Material I	Material II
Elastic modulus / MPa	32 000	32 400
Density / ($\text{kg}\cdot\text{m}^{-3}$)	2 450	1 190
Yield stress / MPa	1, 4, ∞	100, 400
Hardening modulus / MPa	0	100, 300
Fracture toughness / ($\text{N}\cdot\text{mm}^{-1/2}$)	0.003	0.7

3.1 Dynamic ductile crack branching

In this example, a pre-notched rectangular plate in dynamic tension is tested. Fig.4(a) shows the geometry and boundary conditions of this issue. The traction load of 1 MPa is subjected on the top and bottom surface of the plate with a 50 mm initial crack length. A combination meshing scheme of left semi-part unstructured and right semi-part structured meshes with about 13 539 elements is adopted as shown in Fig.4(b), where the right side of the model is densified randomly with 0.000 4 approximate size quadrilateral elements.

The corresponding material parameters are

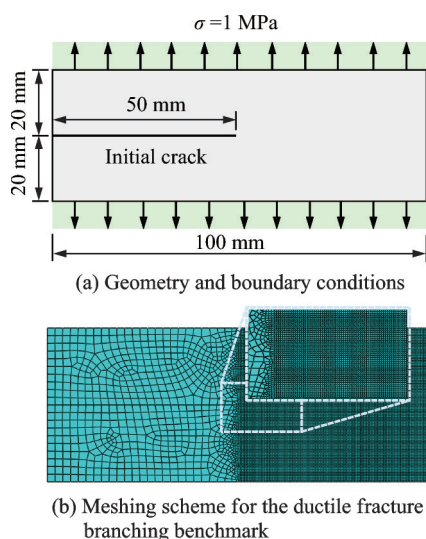


Fig.4 Finite element modeling of the ductile plate

those of Material I presented in Table 1. Three sets of ductile computations are done with different yield stresses, however the hardening is not taken account, in order to study the effect of the yield strength on crack propagation patterns. The length scale l_c is chosen to be 0.002 in this elasto-plastic phase field model, according to the experienced rule in choosing length scale^[23]. And the time step is set to be 10^{-7} s.

To verify the implementation, we compare the brittle fracture pattern predictions from the proposed work and Ref.[24], as shown in Fig.5. When we suppress the elastic threshold and set yield stress as the value of ∞ , two sets of fracture patterns are in good agreement. However, when the elastic threshold is unleashed, the crack propagates and later branches after a longer crack evolution, because the material comes into more resistant. Compared with numerical result of this work, the crack in the result of Ref.[24] diffuses less and propagates longer.

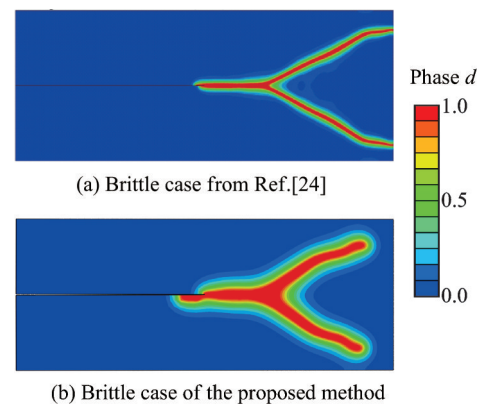


Fig.5 Comparison of brittle fracture pattern predictions from the proposed work and Ref.[24]

In order to investigate the influence of yield strength on the fracture process, Fig.6 shows the predicted phase field with two sets of yield stress (1 MPa and 4 MPa) at different traction levels of 0.5 MPa (50%), 0.6 MPa (60%) and 1 MPa (100%), and their associated equivalent plastic strain can be seen in Fig.7. Compared to the brittle case, the angle of ductile crack branching becomes larger until the branching disappears as the yield stress reduces. This is because the plasticity absorbs the local kinetic energy.

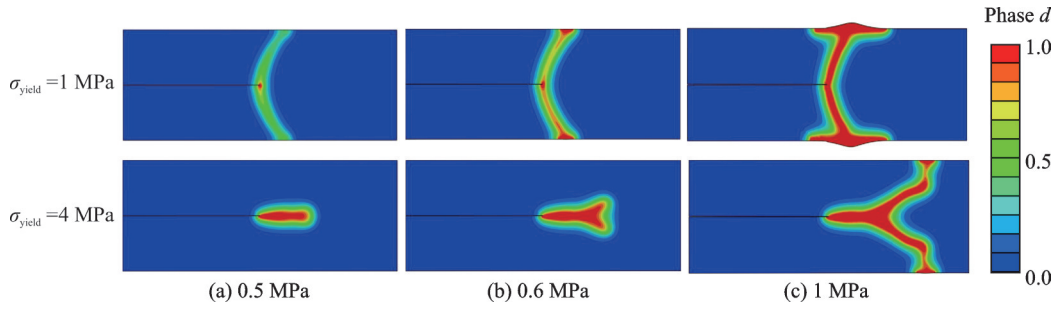


Fig.6 Phase field with two sets of yield stress at different applied loads

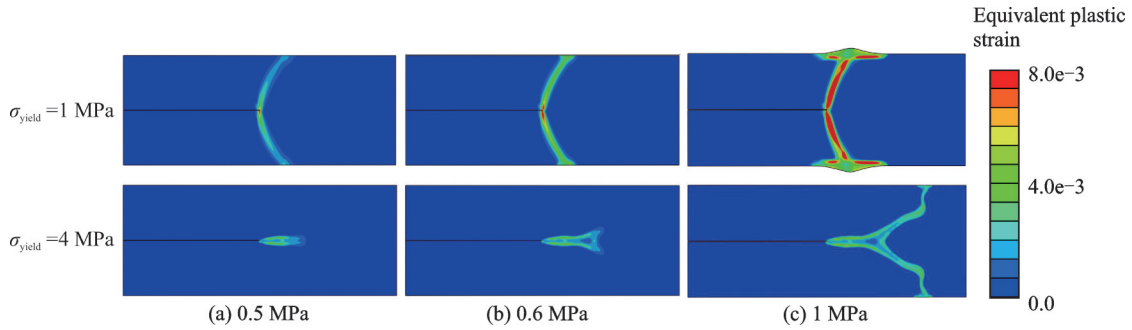


Fig.7 Equivalent plastic strain field with two sets of yield stress at different applied loads

For the case of 1 MPa yield strength, the fracture pattern is the shear mode rather than the tension. It also can be found in Fig.7 that plastic deformation in this case localizes to a band in the vicinity of the fracture zone. However, due to the enhancing effect in the elasto-plastic phase field model, the true level of plastic strain needs to be considered with concentration. Besides, its crack leaking happens at the solid boundary as seen in Figs.6(c) and 7(c), as the kinetic energy cannot be fully dissipated before the cracks propagate at the boundary. Thus, the redundant kinetic waves would basically move along the boundary line to both ends centered on the crack point of the boundary.

In Fig.8, the predicted crack tip velocity is shown as a function of time for different yield stresses. We artificially calculate the position of crack tip as the longest evolution of phase field where its level is more than 0.9. A good agreement is achieved between Ref.[24] and the proposed work. The velocity also remains well below 60% of the Rayleigh wave speed. Besides, an interesting observation can be found that the crack initiation is delayed with the decreasing of the plastic yield stress, which is mostly due to the kinetic energy buffering in the plastic region.

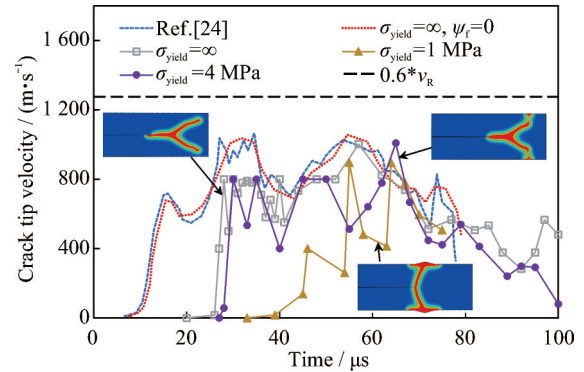


Fig.8 Comparison of crack tip velocity for different yield stresses as a function of time and associated fracture patterns

3.2 Dynamic ductile fracture under shear loading

In this subsection, following the report of Ref.[25], we further consider crack initiation and propagation in the ductile fracture manner under a dynamic shear load. Its material properties are given in Material II of Table 1, and the associated Rayleigh wave speed is 938 m/s. The input geometry and impact conditions (unit is mm) for the simulation are shown in Fig.9.

This model simulates the impact load by imposing a time dependent kinematic velocity on the lower half of the left edge. The impulsive velocity profile is as follows

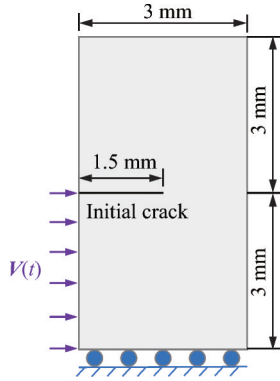


Fig.9 A edge cracked plate under time dependent impact condition

$$V(t) = \begin{cases} \frac{t}{t_0} V_0 & t \leq t_0 \\ V_0 & t > t_0 \end{cases} \quad (25)$$

where $V_0 = 40$ m/s and the rising time $t_0 = 0.1 \mu\text{s}$. The total computing time duration and time step size are $7 \mu\text{s}$ and $0.01 \mu\text{s}$, respectively. This set can make the prescribed rising time cover the time increment size. The concerning part is meshing with 0.03 size quadrilateral elements, and thus the length scale l_c is set to be 0.15.

Fig.10(a) presents the coordinate demonstrating the crack paths. The simulated crack paths with Elastic behavior, Plastic_Y100 (yield stress of 100 MPa, hardening modulus of 100 MPa), and Plastic_Y400 (yield stress of 400 MPa, hardening modulus of 300 MPa) are given in Fig.10(b). Their associated fracture patterns described using phase field are shown in Fig.11. It can be seen that the elastic crack path of phase field simulation is almost within the A-FEM's results range^[25], although crack path at the X -coordinate range of 0.3—0.7 mm is slightly over-predicted. For the plastic problem, ductile cracks propagate towards the lower half of the part, within the distance level of 0.4 mm. The both predicted ductile initiation crack angles are less than elastic initiation crack angle. And besides, the crack in the Plastic_Y100 case does not fully penetrate over the plate due to the kinetic energy buffering in the plastic region.

Fig.12(a) compares the simulated elastic actual crack length (from initiation crack tip to transient crack tip position) against results in Ref.[25]. They are in good agreement except that the crack length is

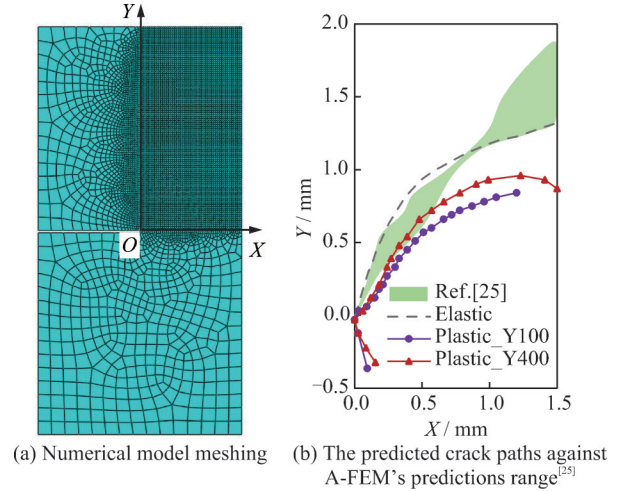


Fig.10 Phase field predicted crack paths

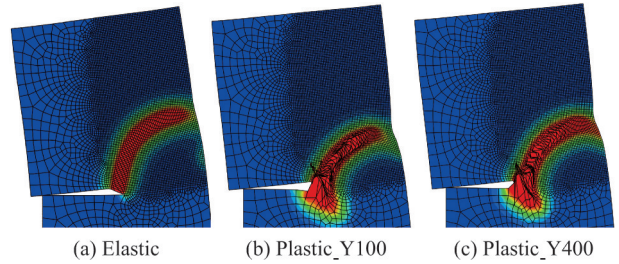


Fig.11 Phase field simulated fracture patterns of elastic and plastic behaviors related to crack paths in Fig.10(b)

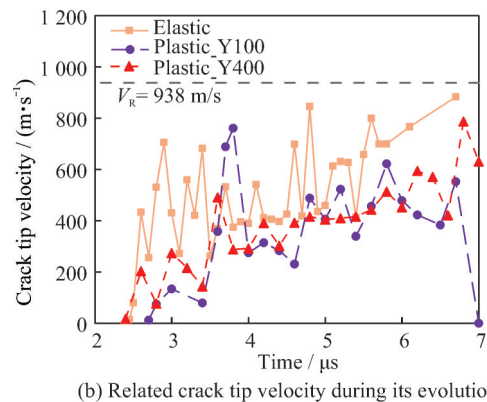
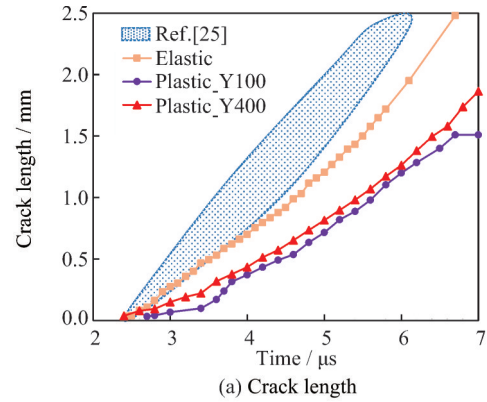


Fig.12 Dynamic crack information analyzed by the ductile phase field

somehow under-predicted slightly. This is because the crack propagation is controlled by the driving force based on the calculated energy in the displacement field, instead of the strength criteria used in A-FEM. The slopes of these curves in Fig.12(a) indicate the instantaneous crack evolution velocity as shown in Fig.12(b). The similar phenomenon can be found that, to a certain extent, the absorption of local kinetic energy in plastic region prevents the crack initiation and propagation as demonstrated in Subsection 3.1. In addition, the predicted speed of these all cracks is significantly smaller than the Rayleigh wave speed.

4 Conclusions

The phase field formulation is extended and demonstrated for the ductile fracture to the dynamic case. This present elasto-plastic version of the phase-field model is implemented within the framework of the staggered implicit dynamic time integration strategy. We note that, the staggered scheme provides efficiency and flexibility, especially when the dynamic crack evolution typically requires time steps of order the Courant number.

With the help of this dynamic elasto-plastic phase field method, we have compared brittle and ductile behaviors by performing numerical experiments for transient crack propagation as well as its branching. An observation has been made in the first numerical test that a high yield stress leads to a perpendicular tensile fracture, while the crack tends to be a tilted angle for low yield stress values. The natural reason is that the material plasticity buffers the local kinetic energy. This phenomenon is also confirmed by the benchmark test in Subsection 3.2, where it is also seen that the ductile crack initiates later and propagates slower compared to the brittle crack.

However, it is not still enough to fully understand the influence of length scale on fracture patterns as well as load bearing capacity. If this issue can be solved, it would be advantageous to further extend the analysis to even rate dependent materials, such as a rate dependent toughness, delayed

damage and viscoelasticity material behavior, compared to other simulation techniques, including extended finite element method, augmentation method, finite fracture mechanics, etc.

References

- [1] DONGEN B V, OOSTRUM A V, ZAROUCHAS D. A blended continuum damage and fracture mechanics method for progressive damage analysis of composite[J]. *Composite Structures*, 2018, 184: 512-522.
- [2] IARVE E V, HOOS K H, NIKISHKOV Y, et al. Discrete damage modeling of static bearing failure in laminated composites[J]. *Composites Part A: Applied Science and Manufacturing*, 2018, 108: 30-40.
- [3] BUDARAPUA P R, REINOSOB J, PAGGI M. Concurrently coupled solid shell based adaptive multi-scale method for fracture[J]. *Computer Methods in Applied Mechanics and Engineering*, 2017, 319: 338-365.
- [4] WANG L, SU H, ZHOU K. A phase-field model for mixed-mode cohesive fracture in fiber reinforced composites[J]. *Computer Methods in Applied Mechanics and Engineering*, 2024, 421: 116753.
- [5] HAO L, YU H, ZHU S, et al. A mode-adjustable phase-field model for brittle fracture by regulating distortional crack driving energy[J]. *Engineering Fracture Mechanics*, 2022, 276: 108920.
- [6] SHI Q, YU H, GUO L, et al. A phase field model with plastic history field for fracture of elasto-plastic materials[J]. *Engineering Fracture Mechanics*, 2022, 268: 108447.
- [7] YU H, HAO L, SHEN R, et al. A phase field model with the mixed-mode driving force of power-law relation[J]. *Engineering Fracture Mechanics*, 2022, 224: 108265.
- [8] WU J Y. A unified phase-field theory for the mechanics of damage and quasi-brittle failure[J]. *Journal of the Mechanics and Physics of Solids*, 2017, 103: 72-99.
- [9] WU J Y, NGUYEN V P. A length scale insensitive phase-field damage model for brittle fracture[J]. *Journal of the Mechanics and Physics of Solids*, 2018, 119: 20-42.
- [10] MANDAL T K, NGUYEN V P, WU J Y. A length scale insensitive anisotropic phase field fracture model for hyperelastic composites[J]. *International Journal of Mechanical Sciences*, 2020, 188: 105941.
- [11] FENG Y, FREDDI F, LI J, et al. Phase-field model for 2D cohesive-frictional shear fracture: An energetic

- formulation[J]. *Journal of the Mechanics and Physics of Solids*, 2024, 189: 105687.
- [12] FENG Y, LI J. Phase-field cohesive fracture theory: A unified framework for dissipative systems based on variational inequality of virtual works[J]. *Journal of the Mechanics and Physics of Solids*, 2022, 159: 104737.
- [13] FENG Y, LI J. Phase-field method with additional dissipation force for mixed-mode cohesive fracture[J]. *Journal of the Mechanics and Physics of Solids*, 2022, 159: 104693.
- [14] BAKTHEER A, MARTÍNEZ-PAÑEDA E, AL-DAKHEEL F. Phase field cohesive zone modeling for fatigue crack propagation in quasi-brittle materials[J]. *Computer Methods in Applied Mechanics and Engineering*, 2024, 422: 116834.
- [15] HAGEMAN T, MARTÍNEZ-PAÑEDA E. A phase field-based framework for electro-chemo-mechanical fracture: Crack-contained electrolytes, chemical reactions and stabilisation[J]. *Computer Methods in Applied Mechanics and Engineering*, 2023, 415: 116235.
- [16] QUINTEROS L, GARCÍA-MACÍAS E, MARTÍNEZ-PAÑEDA E. Electromechanical phase-field fracture modelling of piezoresistive CNT-based composites[J]. *Computer Methods in Applied Mechanics and Engineering*, 2023, 407: 115941.
- [17] DUDA F P, CIARBONETTI A, SANCHEZ P J, et al. A phase field/gradient damage model for brittle fracture in elastic-plastic solids[J]. *International Journal of Plasticity*, 2014, 65: 269-296.
- [18] AMBATI M, GERASIMOV T, DE LORENZIS L. Phase-field modeling of ductile fracture[J]. *Computational Mechanics*, 2015, 55: 1017-1040.
- [19] AMBATI M, KRUSE R, DE LORENZIS L. A phase-field model for ductile fracture at finite strains and its experimental verification[J]. *Computational Mechanics*, 2016, 57: 149-167.
- [20] FANG J, WU C, LI J, et al. Phase field fracture in elasto-plastic solids: Variational formulation for multi-surface plasticity and effects of plastic yield surfaces and hardening[J]. *International Journal of Mechanical Sciences*, 2019, 156: 382-396.
- [21] GUAN W, BHOWMICK S, GAO G, et al. A phase-field modelling for 3D fracture in elasto-plastic solids based on the cell-based smoothed finite element method[J]. *Engineering Fracture Mechanics*, 2021, 254: 107920.
- [22] MOLNÁR G, GRAVOUIL A, SEGHIR R, et al. An open-source Abaqus implementation of the phase-field method to study the effect of plasticity on the instantaneous fracture toughness in dynamic crack propagation[J]. *Computer Methods in Applied Mechanics and Engineering*, 2020, 365: 113004.
- [23] WU J Y. On the unified phase-field theory for damage and failure in solids and structures: Theoretical and numerical aspects[J]. *Chinese Journal of Theoretical and Applied Mechanics*, 2021, 53(2): 301-329.
- [24] BORDEN M J, VERHOUSEL C V, SCOTT M A, et al. A phase-field description of dynamic brittle fracture[J]. *Computer Methods in Applied Mechanics and Engineering*, 2012, 217/218/219/220: 77-95.
- [25] JUNG J, YANG Q D. A two-dimensional augmented finite element for dynamic crack initiation and propagation[J]. *International Journal of Fracture*, 2017, 203: 41-61.

Acknowledgement This work was supported by the National Natural Science Foundation of China (No. 12302176).

Authors Dr. MA Xueshi received his Ph.D. degree in engineering mechanics from State Key Laboratory of Mechanics and Control of Mechanical Structures, Nanjing University of Aeronautics and Astronautics in 2020. During the period of doctoral study, he also studied and did the research as a visiting student in College of Engineering, University of Miami, United States, from 2016 to 2018. His research focuses on damage and fracture mechanics of composite materials, advanced fracture numerical method and marine equipment. Prof. WANG Jia received the B.S. and M.S. degrees in mechanical engineering and automation from Jiangsu University of Science and Technology (JUST) in 2002 and 2005, respectively. From 2002 to present, he has been with the School of Mechanical Engineering, JUST, where he is currently a full professor and deputy director of Jiangsu JMRH Innovation Platform of Deepsea Shipping Transport Key Technology. His research interests are electromechanical control theory and its application on marine equipment.

Author contributions Dr. MA Xueshi designed the study, compiled the models, conducted the analysis, interpreted the results and wrote the manuscript. Mr. WANG Gangyao contributed to the data and figures. Prof. WANG Jia provided the discussion and background of the study. All authors commented on the manuscript draft and approved the submission.

Competing interests The authors declare no competing interests.

(Production Editor: WANG Jing)

用于塑性断裂过程分析的动态相场法

马学仕, 王刚耀, 王 佳

(江苏科技大学机械工程学院, 镇江 212100, 中国)

摘要:相比描述断裂过程的离散数值方法,近期兴起的相场法能够基于连续介质力学框架模拟裂纹扩展,进而避免了离散数值方法中采用的裂纹跟踪算法,使得断裂计算更加简便。本文将弹塑性相场理论与隐式有限元列式结合,试图准确有效地分析动态塑性断裂过程。该弹塑性动态相场法遵循热力学基本原理,基于J2塑性理论捕获塑性材料特征,包括塑化、塑性断裂过程中裂纹萌生、扩展、分叉与汇聚。采用子问题交错迭代时间积分法处理位移场和相场耦合的控制方程,最终编译形成弹塑性动态相场单元,并将该相场单元融入商业有限元软件框架中,进而求解该非线性问题。为验证弹塑性动态相场方法的可靠性,文中给出若干塑性结构断裂分析算例,并得到合理准确的结果。该方法有望在工程弹塑性结构断裂破坏分析领域提供技术支持。

关键词:隐式动力学分析;塑性断裂;弹塑性列式;相场法;复杂裂纹模式